



**HAL**  
open science

## On the plastic deformation of soda-lime glass - a Cr<sup>3+</sup> luminescence study of densification

Antoine Perriot, Etienne Barthel, Guillaume Kermouche, Gilles Querel,  
Damien Vandembroucq

► **To cite this version:**

Antoine Perriot, Etienne Barthel, Guillaume Kermouche, Gilles Querel, Damien Vandembroucq. On the plastic deformation of soda-lime glass - a Cr<sup>3+</sup> luminescence study of densification. *Philosophical Magazine*, 2011, 91 (7-9), pp.1245-1255. 10.1080/14786435.2010.491808 . hal-00495337

**HAL Id: hal-00495337**

**<https://hal.science/hal-00495337>**

Submitted on 25 Jun 2010

**HAL** is a multi-disciplinary open access archive for the deposit and dissemination of scientific research documents, whether they are published or not. The documents may come from teaching and research institutions in France or abroad, or from public or private research centers.

L'archive ouverte pluridisciplinaire **HAL**, est destinée au dépôt et à la diffusion de documents scientifiques de niveau recherche, publiés ou non, émanant des établissements d'enseignement et de recherche français ou étrangers, des laboratoires publics ou privés.

## RESEARCH ARTICLE

### On the plastic deformation of soda-lime glass – a Cr<sup>3+</sup> luminescence study of densification

A. Perriot<sup>a</sup>, E. Barthel<sup>a\*</sup>, G. Kermouche<sup>b</sup>, G. Quérel<sup>c</sup> and D. Vandembroucq<sup>d</sup>

<sup>a</sup>*Unité Mixte de Recherche CNRS/Saint-Gobain, 39 Quai Lucien Lefranc, 93303 Aubervilliers Cedex, France.*; <sup>b</sup>*Université de Lyon, ENI Saint-Etienne, LTDS, UMR5513, 58 rue Jean Parot, 42023 Saint-Etienne, France.*; <sup>c</sup>*Saint-Gobain Recherche, 39 Quai Lucien Lefranc, 93303 Aubervilliers Cedex, France.*; <sup>d</sup>*Laboratory PMMH, ESPCI, 10 rue Vauquelin, 75231 Paris Cedex 05, France.*

(v4.4 released ??? november 2009)

Silicate glasses are known to experience an anomalous plastic behavior at micron-scale: 1) they exhibit densification when flowing plastically and 2) hydrostatic pressure affects the yield point. We have previously shown (A. Perriot *et al.* *J. Am. Ceram. Soc.* 89 (2006) 596) that densification maps are useful to infer a reliable constitutive law for the plastic response of silicate glasses. It is shown here that for soda-lime glass Cr<sup>3+</sup> luminescence microspectroscopy may be used for that purpose. We also show that the constitutive law we have previously developed for amorphous silica provides a qualitative description of normal glasses although it is unable to account for the finer details. More work is needed to quantitatively model normal-glass plasticity at the continuum length-scale.

**Keywords:** Plasticity, Glass, Indentation, Constitutive model

#### 1. Introduction

Silicate glasses are considered as the archetype of brittle materials. However, various experiments [1–3] have shown that they exhibit plastic response in highly confined geometries (Diamond-Anvil Cell (DAC) [4, 5], indentation [1, 6],...). Moreover, this so-called “micro-ductile” behavior departs from the ubiquitous crystalline plasticity which is triggered by shear and conserves volume. Indeed silicate glasses exhibit densification under purely hydrostatic loading [7], but they also densify during plastic shear flow [6]. The permanent volumetric strain (densification) is known to saturate [8, 9] at a value which depends on the glass composition. The less polymerized, the smaller the maximum possible densification. It amounts to a few percents for highly modified glasses [10], which are commonly called, for obvious historical reasons, “normal” glasses. It can reach as much as 20% in the case of amorphous silica [9], which is the archetype of the so-called “anomalous” glasses.

For predictive purposes, it is useful to obtain a constitutive equation for the plastic deformation of amorphous silicates. To take densification into account, a few authors have proposed a Drucker-Prager-like plastic criterion [9, 11]. The model parameters were adjusted using a trial-and-error approach based on Finite Element (FE) analysis of indentation experiments. This is a delicate task, because indentation is a highly inhomogeneous loading and indentation curves [11, 12] or residual

---

\*Corresponding author. Email: etienne.barthel@saint-gobain.com

indent profile [11] provide a very limited set of data to fit a complex constitutive equation. A richer set of data is required but due to the brittle nature of amorphous silicates, which exhibit plasticity only at the micron-scale, these experiments must be performed at the micron-scale.

Previously [13], we used Raman micro-spectroscopy to provide densification maps of indents in amorphous silica. We also proposed a constitutive law for the elasto-plastic response of amorphous silicates. This model, which is inspired by porous materials, takes into account the hydrostatic hardening behavior of silica, which has been independently identified with the help of Diamond Anvil Cell experiments [14]. Starting from this constitutive law, a good agreement with the experimental indentation-induced densification maps [13] is obtained.

However, for silica, the measurement of the densification maps relies on the  $D_2$ -line shift. Indeed the relation of this shift with density has been reported in details in the literature [4, 7, 15]. Unfortunately, for normal silicate glasses, spectral bands appear with the addition of modifiers and they tend to conceal the  $D_2$  band. As a result, another way to characterize material density at the local scale is required.

Transition and rare-earth ions have long been used to characterize the structural changes in densified glasses [16]. Quérel has studied the evolution of the luminescence spectrum of  $Cr^{3+}$  ion in doped silicate glasses [17, 18]. The results suggest that luminescence could be used as a local probe for density. In the present work, we performed a microspectroscopic mapping of the  $Cr^{3+}$  ion luminescence spectrum of indented areas in two  $Cr^{3+}$ -doped commercial-grade glass samples. We show that  $Cr^{3+}$  luminescence is a promising way to extend the measurement of residual densification map to other silicate glasses. In addition, the resulting maps are compared to numerical predictions based on the constitutive model we have previously developed for silica [19], demonstrating rough agreement. However, it is shown that for a full prediction of the shape of the density distribution, additional features must be included in the constitutive law.

## 2. Experimental procedure

For the samples, two commercial bottles were fused into discs. The composition of the glasses, labelled G1 and G2, are about 71%  $SiO_2$ , 12%  $Na_2O$  and 10%  $CaO$  (Table 1), which is a typical industrial formulation of soda-lime glass. Plates of dimension  $8 \times 8 \times 0.5$  cm<sup>3</sup> were cut out from these discs and polished. The residual stresses induced by polishing were relaxed by annealing and 2-kg Vickers indentations were performed on the plates.

We used a Raman microspectroscopy device (Thermonicolet) including a 25 mW, 532 nm laser, under a  $\times 100$  objective. The laser beam was focused on the surface using a confocal setup. The excited volume of glass was approximately  $2 \times 2 \times 2$   $\mu m^3$ . We performed surface mappings on three indents of each type of glass. A typical map consists in a collection of 52 spectra taken with a 10  $\mu m$ -spacing on half views of indents. For each spectrum, the luminescence signal was accumulated during 1 s, to be compared with the 900 s necessary to obtain an equivalent spectrum while performing Raman microspectroscopic mapping of indented silica [13].

## 3. Results

Figure 1 contrasts a spectrum obtained in the center of an indent with a reference spectrum acquired away from the indents. Between 12,163 and 14,924  $cm^{-1}$ , the luminescence spectrum of a  $Cr^{3+}$ -doped glass consists of two bands: a wide band

centered around  $12,800 \text{ cm}^{-1}$  and a narrower band around  $14,550 \text{ cm}^{-1}$ , forming a shoulder on the first. According to Qu erel [17, 18], these two bands respectively correspond to the transitions  ${}^4T_2 \rightarrow {}^4A_2$  and  ${}^2E \rightarrow {}^4A_2$ . This lineshape results from a wide distribution of  $\text{Cr}^{3+}$  sites with a range of crystal field environments [20, 21].

Let us consider the Tanabe-Sugano diagram for  $\text{Cr}^{3+}$  ion in an octahedral site (Fig. 2).  $Dq/B$  quantifies the overall influence of the crystal field since  $Dq$  is related to the crystal field intensity and  $B$  to the covalent nature of the  $\text{Cr}^{3+}$  atomic bonds. The energy of the  ${}^4T_2$  level crosses the  ${}^2E$  level for  $Dq/B \simeq 2$ . As both  ${}^4T_2$  and  ${}^2E$  levels comply with the transition rules, they are both emissive. As a result the Tanabe-Sugano diagram suggests that when  $Dq/b < 2$ , the luminescence transition is  ${}^4T_2 \rightarrow {}^4A_2$ , while it is  ${}^2E \rightarrow {}^4A_2$  for  $Dq/B > 2$ .

Experiments performed with a DAC [18] have shown that under hydrostatic compression  $\text{Cr}^{3+}$ -doped silicate glasses exhibit two main pattern changes: 1) the intensity of the  ${}^2E \rightarrow {}^4A_2$  band increases with respect to the  ${}^4T_2 \rightarrow {}^4A_2$  band and 2) it shifts to lower frequencies. These phenomena were interpreted as a local compression of the  $\text{Cr}^{3+}$  sites [17]. Indeed, the hydrostatic pressure enhances the crystal field and increases  $Dq/B$ . With increasing hydrostatic pressure,  $\text{Cr}^{3+}$  sites shrink,  $Dq/B$  increases and the intensity ratio  $({}^2E \rightarrow {}^4A_2)/({}^4T_2 \rightarrow {}^4A_2)$  increase. As a result a shift to *lower frequencies* is observed, due to the increase of the population of  ${}^2E \rightarrow {}^4A_2$  sites with pressure.

The  ${}^2E \rightarrow {}^4A_2$  band positions and relative intensities are markers of the local volume distortion of the material. Experimentally, these two markers were evaluated through spectral deconvolution: the high frequency side of the  ${}^4T_2 \rightarrow {}^4A_2$  band was fitted with a gaussian, providing a good estimate for the band height. This gaussian was used as a baseline which was subtracted to the spectrum. Finally the  ${}^2E \rightarrow {}^4A_2$  band was fitted with a Pearson IV function for band height and position.

The resulting maps are presented on Fig. 3. The lines satisfy the symmetries of the indenter. Moreover, notice that for both indicators and both samples the center of the indent does appear as the most densified part of the indented area: as the laser spot moves nearer to the center of the indent, the  ${}^2E \rightarrow {}^4A_2$  band shifts towards low frequencies and its relative intensity increases.

#### 4. Density estimation

Qu erel [17] has given a relation between the  ${}^2E \rightarrow {}^4A_2$  band shift and the average hydrostatic pressure applied on several glass samples of different compositions. **Since this approximate relation is otherwise unpublished, we give some more details here.** It is assumed that shear does not affect the  ${}^2E \rightarrow {}^4A_2$  band position and that the bulk modulus remains reasonably unchanged with density. If  $\alpha$  is the band shift per unit of pressure and  $B$  the bulk modulus of the material, then, the densification as a function of the band shift  $\Delta\nu$  is given by

$$\frac{\Delta\rho}{\rho} = \frac{\Delta\nu}{\alpha B} \tag{1}$$

In the case of a model 60%- $\text{SiO}_2$ -20%- $\text{Na}_2\text{O}$ -20%- $\text{CaO}$  soda-lime glass,  $\alpha$  is evaluated to about  $12.5 \text{ cm}^{-1}/\text{GPa}$  towards low frequencies, while  $B \simeq 39 \text{ GPa}$ , for a Young's modulus equal to 70 GPa and a Poisson ratio equal to 0.2.

Then, with equation (1), we obtain the densification maps presented on Fig. 4. We notice that the maximum densification is about 3 to 4%. These values are

reasonably consistent with the “normality” of the samples. In comparison, Ji et al [22] report a maximum densification equal to about 5-6% for window (soda-lime) glass, which is consistent with the present results.

Clearly Eq. 1 provides only a rough evaluation and further refinements are needed if the method is to be used more extensively. At the present stage of development of the method it is difficult to provide error bars but, given the crudeness of the approximation, we believe that the qualitative agreement with previous results for similar glasses [22] is encouraging.

### 5. Iso-density contours

We now discuss the shape of the iso-density contours. Fig. 3 demonstrates that for the silicate glasses G1 and G2 the contours are convex. This shape strongly contrasts with the concave iso-density contours observed on Vickers-indented silica (Figure 5). Note that for silica (bottom), the concave contours result in a star-shaped pattern, while a much more circular figure is revealed in the case of soda-lime glass. The density contrast between the Vickers edges and faces is less marked for soda-lime glass than for amorphous silica [13]. This result is consistent with the fact that soda-lime glasses are normal, in contrast to silica. Indeed, optical observations by Hagan and Van der Zwaag [10], as well as a rough model by Yoffe [23], demonstrate that the densified area under the indenter is expected to be more regular and spherical with increasing glass normality. **These contrasted shapes for the iso-density contours of normal and anomalous glasses is the main result of the paper. It is to be emphasized that it should be robust against uncertainties in the quantitative conversion between spectroscopic features and density.**

### 6. Finite element analysis of the indentation-induced densification process

In a previous paper [19], we have shown that a constitutive model based on the mechanics of porous materials can be used to predict indentation-induced densification maps on silica. In this section we test the predictions of the model on the maps shown in the previous sections. For a similar normal glass, the densification under high pressure has been measured recently [22].

Let us just recall the main features of this constitutive model. In compression, the yield criterion is

$$f(\sigma_{ij}) = \left(\frac{q}{q_c}\right)^2 + \left(\frac{p}{p_c}\right)^2 - 1 \tag{2}$$

where  $p_c$  is the (hydrostatic) plastic limit in pure hydrostatic loading and  $q_c$  the (shear) plastic limit in pure deviatoric loading. This form of the yield criterion allows us to consider an associative flow rule. The densification-induced hardening is modeled by taking into account an increase of the hydrostatic limit  $p_c$  with the plastic densification of the material. This plastic densification implies that a part of the free volume disappears under hydrostatic pressure. This hydrostatic hardening is thus directly related to the free volume fraction  $\Phi$  which decreases from the initial free volume  $\Phi_0$  to zero (saturation). Similarly to the compaction of powders, the irreversible evolution of free volume is given by

$$\dot{\Phi} = (1 - \Phi)Tr(\dot{\epsilon}^p) \tag{3}$$

The densification-induced hardening data of Vandembroucq et al [14] have been used for silica whereas the densification-induced hardening data of Ji et al [22] have been chosen for the window (soda-lime) glass. The shear limit  $q_c$  for soda-lime glass has been quantified from nanoindentation data, using the methodology presented previously [19]. The set of parameters identified for these two materials are summarized in table 2.

Calculations have been performed with the Finite Element Software Systus [24] using 3D elements and using a large displacement / large strain option (updated Lagrangian formulation, logarithmic strain). The boundary and loading conditions are similar to those proposed by Giannakopoulos *et al.* [25]. The resulting densification maps are plotted in Figure 6. For both silica and soda-lime glass, the densification gradient is well reproduced. Moreover, the curvature of the iso-densification lines of amorphous silica (b) are consistent with the experimental micro-raman results [13]: the density is higher under the edges than under the faces of the Vickers indenter, leading to star-shaped iso-densification lines. However, the iso-densification lines of soda-lime glass are also star-shaped which is in strong contrast with the new experimental results (Fig 5) presented here. It is thus clear that our constitutive model performs better to model the plastic deformation for silica than for normal glasses.

## 7. Conclusion

We have used the luminescence of  $\text{Cr}^{3+}$ -doped soda-lime glasses to evaluate the distribution of the residual indentation-induced densification in normal glasses. Our results are consistent with previous results in the literature [10, 23]. These results stress the potential of  $\text{Cr}^{3+}$  as a local marker of density. Using this marker, we have extended our method to propose a constitutive law for the plastic deformation of normal silicate glasses. Moreover, considering the reduced acquisition time necessary to obtain reasonable signal-to-noise ratios, this marker should drastically reduce the time necessary to obtain a densification map. For more precise measurements, more extensive data on the correlation between sample density and luminescence spectra would be necessary. They could be obtained with heat-and-pressure densified macroscopic samples of glasses. The effect of the residual elastic shear stress on the spectral patterns should also be explored carefully.

Finally, we have shown that the elastic-plastic constitutive model previously developed for silica is only qualitatively valid for more normal glasses such as soda-lime glasses. The overall density gradient is well accounted for in both cases. However, the calculated iso-densification lines are star-shaped in both cases, whereas the experiments reveal spherical iso-densification lines for soda-lime glasses. Consequently a new constitutive model specifically adapted to the densification behaviour of normal glasses has to be developed.

## 8. Acknowledgments

The authors would like to thank G. Duisit, R. Gy, S. Pelletier and S. Roux for their help, advice and support.

## References

- [1] E. Taylor, Nature 163 (1949) p.323.

- [2] J. Mackenzie, J. Am. Ceram. Soc. 46 (1963) p.461.
- [3] F. Célarié, S. Prades, D. Bonamy, L. Ferrero, E. Bouchaud, C. Guillot and C. Marlière, Phys. Rev. Lett. 90 (2003) p.75504.
- [4] J.M. Mikkelsen Jr. and F. Galeener, J. Non-Cryst. Solids 37 (1980) p.71.
- [5] M. Grimsditch, Phys. Rev. Lett 52 (1984) p.2379.
- [6] F. Ernsberger, J. Am. Ceram. Soc. 51 (1968) p.545.
- [7] H. Sugiura and T. Yamadaya, J. Non-Cryst. Solids 144 (1992) p.151.
- [8] A. Polian and M. Grimsditch, Phys. rev. B 41. (1990) p.6086.
- [9] J. Lambropoulos, S. Xu and T. Fang, J. Am. Ceram. Soc. 79 (1996) p.1441.
- [10] J. Hagan and S.V.D. Zwaag, J. Non-Cryst. Solids 64 (1984) p.249.
- [11] M. Imaoka and I. Yasui, J. Non-Cryst. Solids 22 (1976) p.315.
- [12] K. Xin and J. Lambropoulos, Proc. SPIE 4102 (2000) p.112.
- [13] A. Perriot, V. Martinez, C. Martinet, B. Champagnon, D. Vandembroucq and E. Barthel, J. Am. Ceram. Soc. 89 (2006) p.596.
- [14] D. Vandembroucq, T. Deschamps, C. Coussa, A. Perriot, E. Barthel, B. Champagnon and C. Martinet, J. Phys.: Condens. Matter 20 (2008) p.485221.
- [15] H. Sugiura, R. Ikeda, K. Kondo and T. Yamadaya, J. Appl. Phys. 81 (1997) p.1651.
- [16] N. Soga, K. Hirao, M. Yoshimoto and H. Yamamoto, J. Appl. Phys. 63 (1988) p.4451.
- [17] G. Quérel, *Cristallochimie des éléments traces dans les phases du manteau terrestre – Applications de la spectroscopie de luminescence à haute pression et haute température*, University of Rennes, France, 1997.
- [18] G. Quérel and B. Reynard, Chem. Geol. 128 (1996) p.65.
- [19] G. Kermouche, E. Barthel, D. Vandembroucq and P. Dubujet, Acta Materialia 56 (2008) p.3222.
- [20] M. Yamaga, B. Henderson, K. O'Donell and Y. Gao, Phys. Rev. B 44 (1991) p.4853.
- [21] F. Rasheed, K. O'Donell, B. Henderson and D. Hollis, J. Phys. : Condens. Matter 3 (1991) p.1915.
- [22] H. Ji, V. Keryvin, T. Rouxel and T. Hammouda, Scripta Materialia 55 (2006) p.1159.
- [23] E. Yoffe, Phil. Mag. A 46 (1982) p.617.
- [24] Systus/Sysweld, 2009 in *User's manual* ESI Group.
- [25] A. Giannakopoulos, P. Larsson and R. Vestergaard, Int. J. Solids Structures 31 (1994) p.2679.



| sample | SiO <sub>2</sub> | Na <sub>2</sub> O | CaO    | MgO   | Al <sub>2</sub> O <sub>3</sub> | K <sub>2</sub> O | Fe <sub>2</sub> O <sub>3</sub> | Cr <sub>2</sub> O <sub>3</sub> | TiO <sub>2</sub> , SO <sub>3</sub> |
|--------|------------------|-------------------|--------|-------|--------------------------------|------------------|--------------------------------|--------------------------------|------------------------------------|
| G1     | 70.5 %           | 12.3 %            | 10.4 % | 2.0 % | 2.3 %                          | 890 ppm          | 440 ppm                        | 220 ppm                        | traces                             |
| G2     | 71.6 %           | 12.4 %            | 10.9 % | 1.4 % | 2.1 %                          | 700 ppm          | 320 ppm                        | 200 ppm                        | traces                             |

Table 1. Composition of the samples used in this study. Both are commercial grade Cr<sup>3+</sup>-doped glasses.

|                 | E (GPa) | $\nu$ | $q_c$ (MPa) | $\Phi_0$ |
|-----------------|---------|-------|-------------|----------|
| Silica          | 70      | 0.17  | 7           | 17 %     |
| Soda-lime glass | 75      | 0.22  | 3.5         | 5.5 %    |

Table 2. Set of parameters used for silica and soda-lime glass. These values of initial free volume result in maximum densifications of respectively 20 % and 6 %.

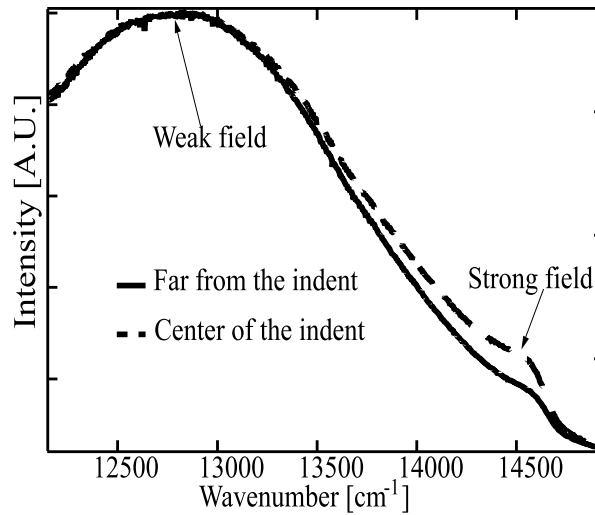


Figure 1. Luminescence spectra of Cr<sup>3+</sup>-doped soda-lime glass. The plain line spectrum was obtained in an unmodified area of the sample, while the dotted line corresponds to the center of the indent (which is expected to be the most densified area).

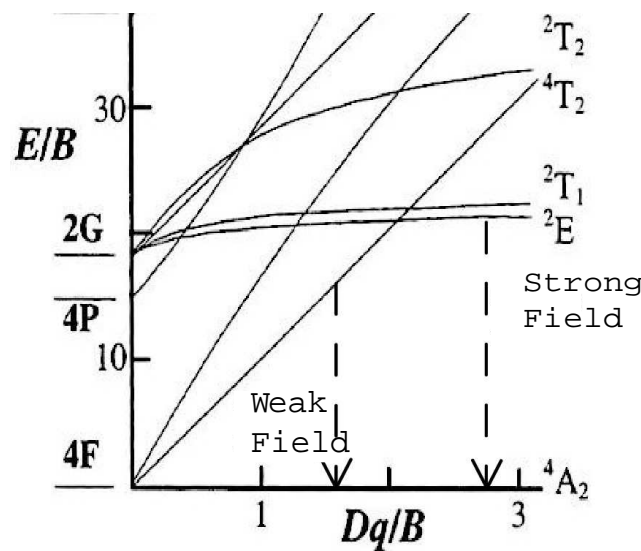


Figure 2. Tanabe-Sugano diagram for Cr<sup>3+</sup> in octahedral symmetry. With increasing influence of the crystal field, the “weak field” Cr<sup>3+</sup>-occupied sites tend to become “strong field” sites.



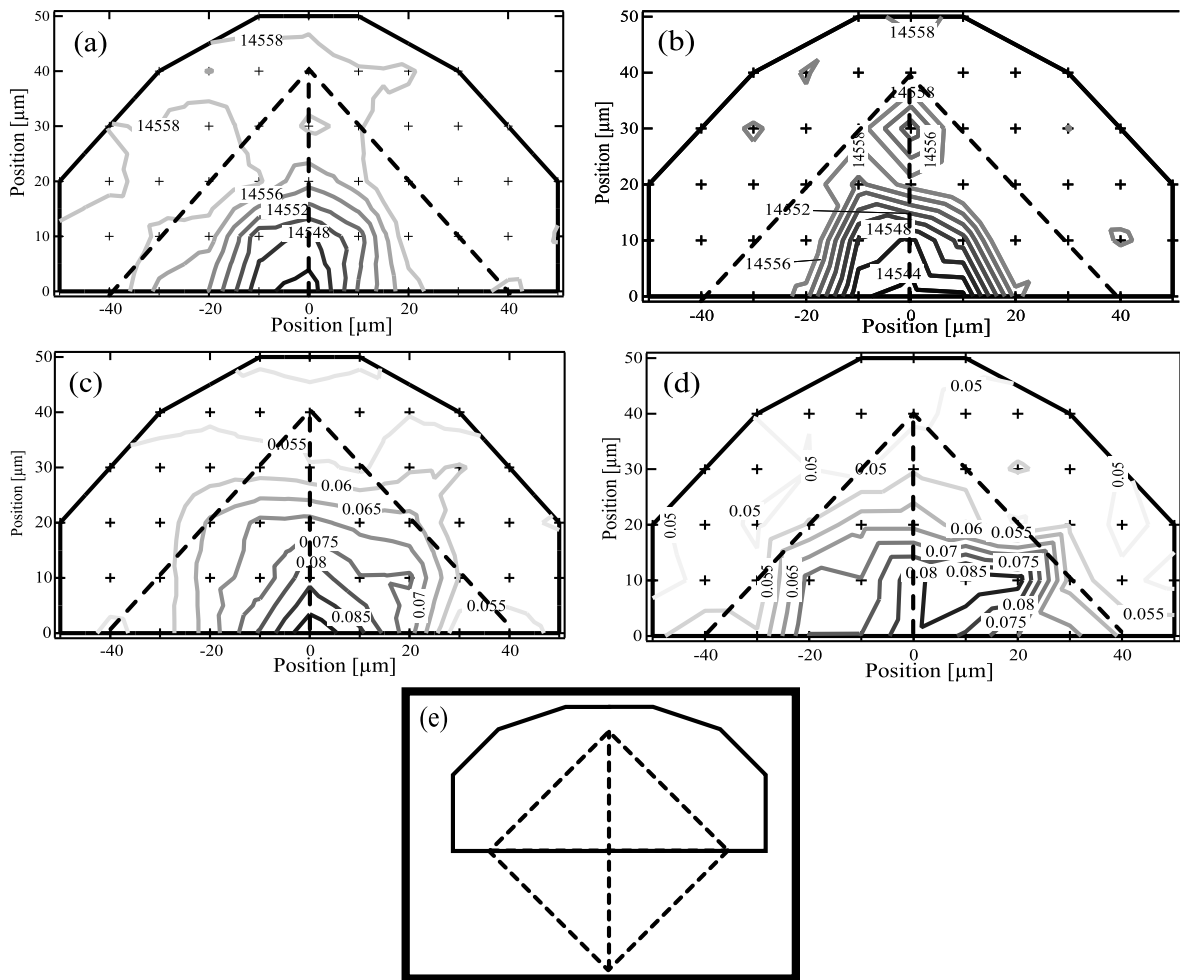


Figure 3. Maps of the spectroscopic features of the  ${}^2E \rightarrow {}^4A_2$  transition over densified areas of glasses G1 (a and c) and G2 (b and d). The densification was obtained by Vickers indentation. The half-view maps (a) and (b) display the peak position and the half-view maps (c) and (d) the peak height normalized to the  ${}^4T_2 \rightarrow {}^4A_2$  band. Numerical values are given in  $\text{cm}^{-1}$  (a and c) and non-dimensional (b and d). Iso-indicator contour lines are shown in grey. The limits of the indents are shown as bold dotted lines and the limits of the scanned area as bold black lines, as sketched in (e). The center of the indent is at coordinates (0;0) and the dark crosses are the measurement positions.

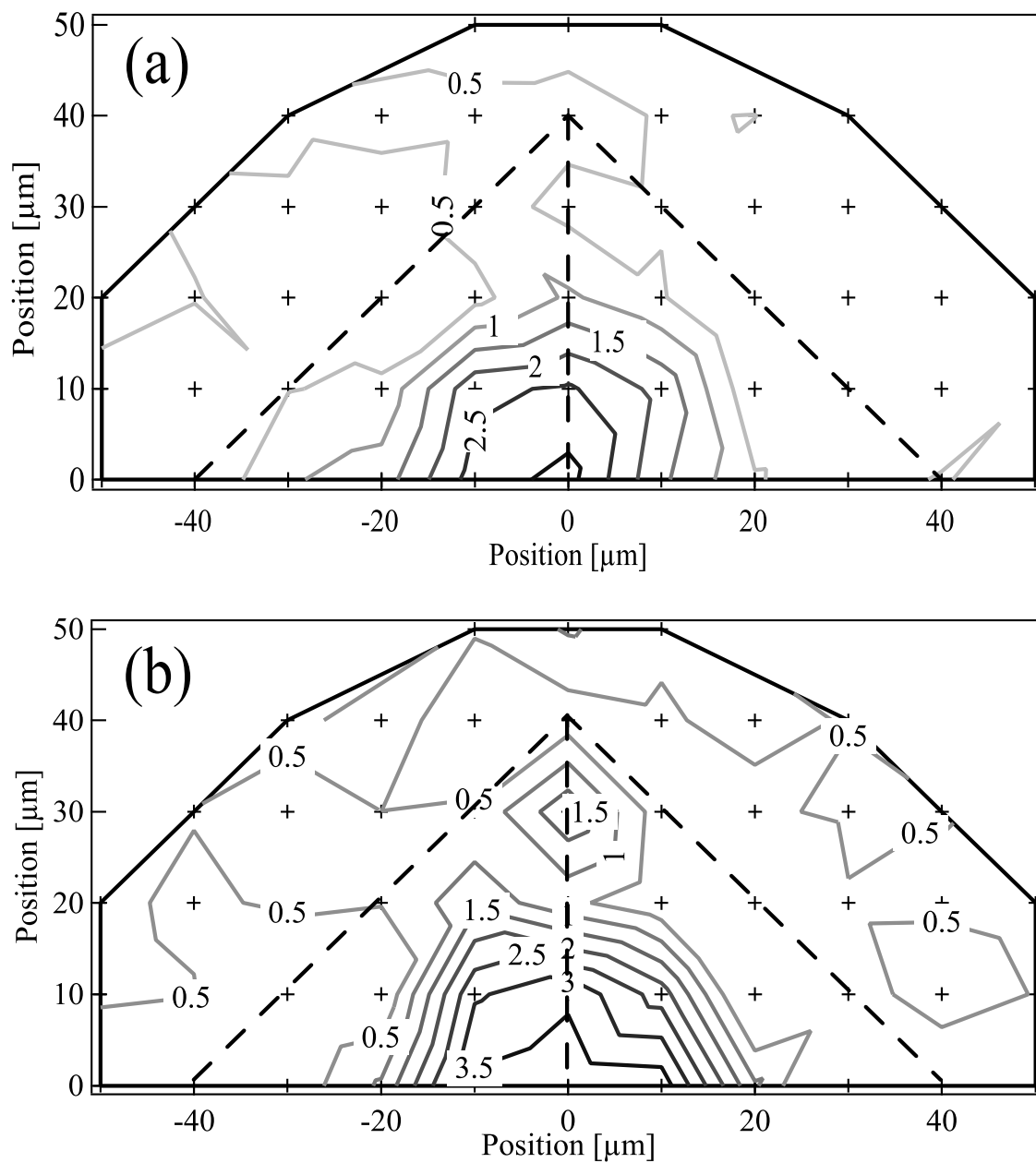


Figure 4. Densification maps for sample G1 (a) and G2 (b) (see text). The increment between iso-density contours is 0.5 %.

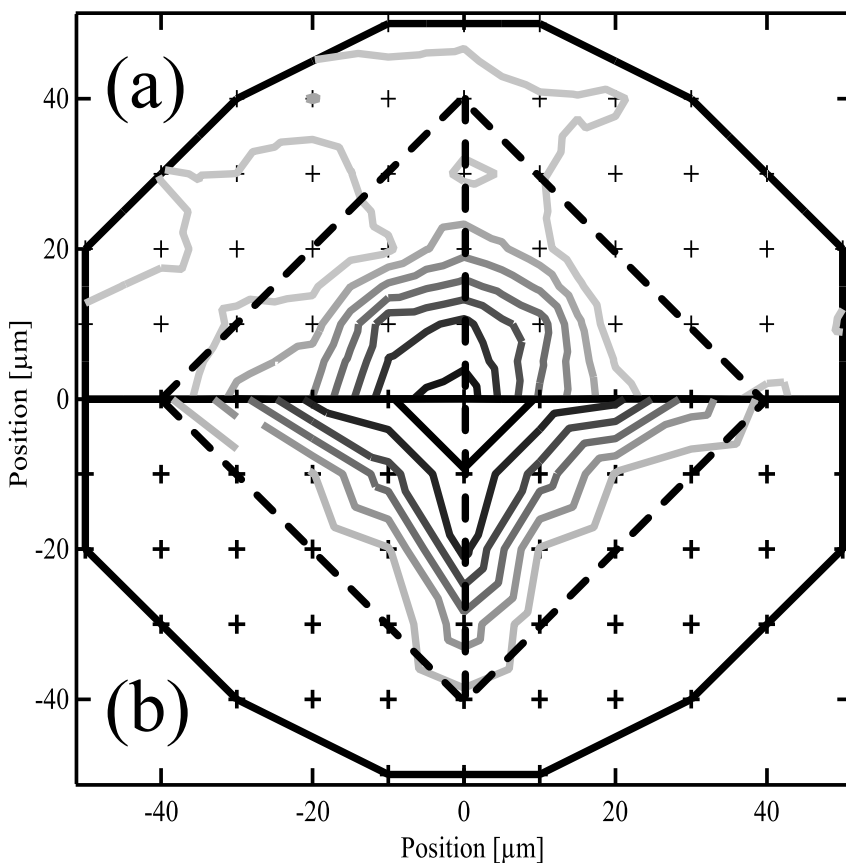


Figure 5. Density maps obtained on sample G1 (a) (iso-density contours with 0.5 % increments) and on amorphous silica (b) (iso-density contours with 2.5 % increments, increasing from outside the contact area to inside). The iso-density contours for the “normal” glass (a) are close to circular while they are star-shaped for silica which is an “anomalous” glass.

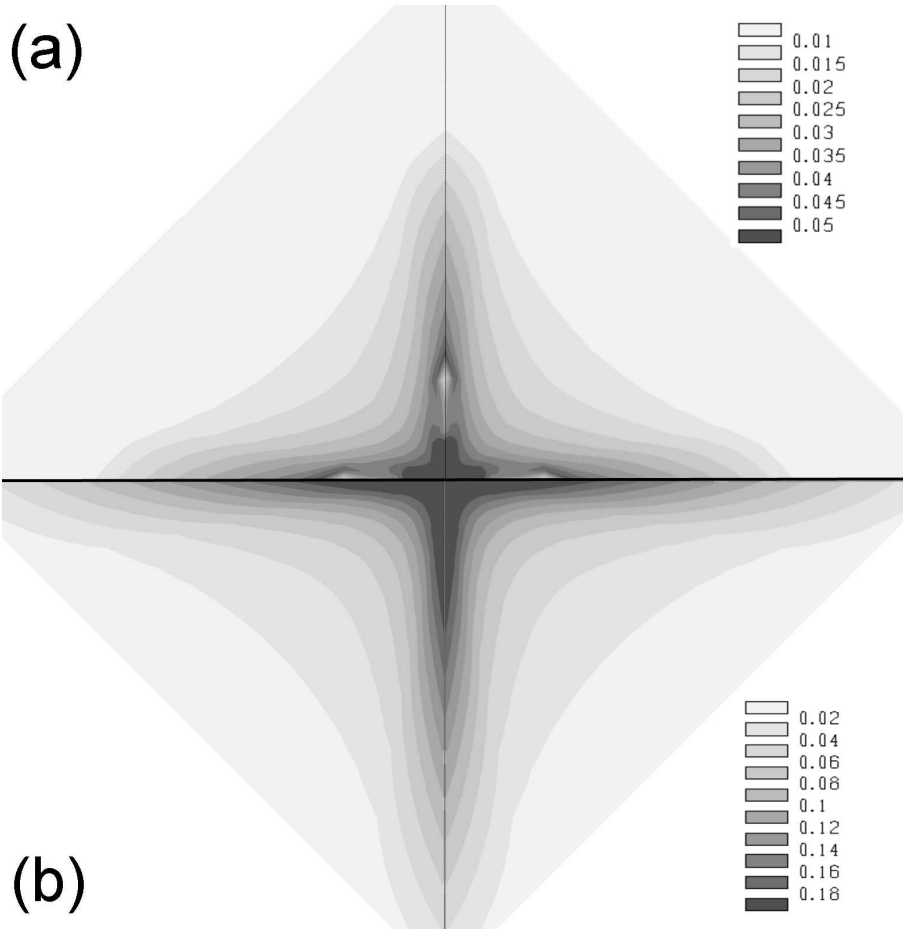


Figure 6. Finite element simulations of the densification maps obtained on soda-lime glass (a) and on amorphous silica (b) with the parameters of Table 2.